The crystal structures of superionic Ag_3SI

2001 J. Phys.: Condens. Matter 13 2295

(http://iopscience.iop.org/0953-8984/13/10/321)

INSTITUTE OF PHYSICS PUBLISHING JOURNAL OF PHYSICS: CONDENSED MATTER

J. Phys.: Condens. Matter **13** (2001) 2295–2316 www.iop.org/Journals/cm PII: S0953-8984(01)17976-2

The crystal structures of superionic Ag_3SI

S Hull[1], D A Keen[1], N J G Gardner[2] and W Hayes[2]

[1] The ISIS Facility, Rutherford Appleton Laboratory, Chilton, Didcot, Oxfordshire OX11 0QX, UK
[2] Clarendon Laboratory, Parks Road, Oxford OX1 3PU, UK

Received 12 October 2000

Abstract

The crystal structures of the four phases of the 'anti-perovskite' superionic conductor Ag_3SI have been investigated by powder neutron diffraction and complex impedance spectroscopy. The high-temperature α-phase is characterized by a random distribution of the two cation species S^{2-} and I^- over the 2(a) positions at 0, 0, 0 and 1/2, 1/2, 1/2 within space group $Im\bar{3}m$. The Ag^+ are found to preferentially occupy the 24(h) trigonal interstices within the anion sublattice, though with significant anisotropy in their thermal vibrations. On quenching from high temperature the disordered cation array is retained, forming the metastable α^*-phase, but there is a significant change in the cation distribution. The Ag^+ are predominantly located in 24(g) sites between the octahedral and tetrahedral cavities, though a significant proportion are found in 48(i) sites close to the 1/4, 1/4, 1/4 position midway between two anions. The latter are displaced by ∼0.7 Å in ⟨110⟩ directions to avoid short cation–anion contacts. Slow cooling from the α-phase followed by prolonged annealing at modest temperatures (∼473 K) stabilizes the β-phase of Ag_3SI, in which long-range ordering of the two cation species lowers the symmetry to $Pm\bar{3}m$. The Ag^+ now occupy 12(h) positions close to half the octahedral sites, such that they do not form close contacts with the larger I^- species. The displacements are in the four ⟨100⟩ directions and towards the tetrahedral sites, with a single Ag^+ randomly occupying one of these four 'split' positions. On cooling, the ionic conductivity is found to drop abruptly by ∼4× at $T = 156(2)$ K at the $\beta \rightarrow \gamma$ transition. High-resolution powder neutron diffraction studies indicate that γ-Ag_3SI possesses a very small rhombohedral distortion of the unit cell. The crystal structure of γ-Ag_3SI (space group $R3$) can be derived from that of the β-phase by long-range ordering of the Ag^+ onto a subset of the displaced octahedral positions and an associated small displacement of the S^{2-} in a ⟨111⟩ direction.

1. Introduction

Superionic compounds are materials which exhibit exceptionally high values of ionic conductivity (typically $\sigma \sim 0.01$–$1\ \Omega^{-1}\ \mathrm{cm}^{-1}$) whilst in the solid state [1]. In general,

the superionic behaviour is associated with the onset of extensive, dynamic disorder of a subset of the constituent ionic species. Silver iodide, AgI, is one of the simplest, yet most widely studied, examples. At 420 K it transforms from the 'normal' insulating β-phase to the superionic α-phase with an increase in the ionic conductivity σ of almost four orders of magnitude (see [2] and references therein). In the α-phase σ has a value $\sim 2\ \Omega^{-1}\ \mathrm{cm}^{-1}$ which increases only slowly with temperature and actually decreases slightly at the melting point of $T_m = 829$ K. Neutron diffraction studies of α-AgI have indicated that the I^- form an essentially rigid body-centred cubic (b.c.c.) sublattice, with the Ag^+ rapidly hopping between the tetrahedrally coordinated positions via the trigonal ones [3, 4]. Many other superionic phases formed by a b.c.c.-structured anion sublattice are known, including α-CuBr [5], β-Ag_2S [6], α-Ag_2Se [7] and γ-Ag_2Te [8, 9] and further examples are observed at elevated pressures (CuCl-III [10] and CuI-VII [11]). However, all the phases listed above are only stable at elevated temperatures and the potential technological applications of superionic compounds require that the superionic transition temperature be reduced to below ambient temperature.

One of the most promising compounds is Ag_3SI, which was first reported in 1965 by Reuter and Hardel [12–14]. At temperatures above 519 K Ag_3SI exists in its α-phase which is characterized by a random distribution of S^{2-} and I^- over the $0, 0, 0$ and $1/2, 1/2, 1/2$ positions of a cubic unit cell with $a \sim 5.0$ Å. The mobile Ag^+ are located predominantly near the octahedral cavities but undergo rapid diffusion along the $\langle 100 \rangle$ directions [15–17]. Samples which are slowly cooled to room temperature undergo an ordering of the two cation species over the 0, 0, 0 and $1/2, 1/2, 1/2$ positions, such that the space group changes from $Im\bar{3}m$ to $Pm\bar{3}m$ [16–18]. The Ag^+ are generally considered to sit close to the octahedral positions but displaced in one of four $\langle 100 \rangle$ directions towards the tetrahedral sites. As such, β-Ag_3SI can be considered to be an 'anti-perovskite' structure. On further cooling a reversible transition to γ-Ag_3SI has been observed at $T \sim 157$ K by specific heat methods [19]. The $\beta \leftrightarrow \gamma$ transition is probably of first order [19], but has been proposed to be due to an ordering of the Ag^+ over the tetrahedral interstices as the symmetry is lowered from cubic to rhombohedral [18–20]. Quenching to room temperature from the α-phase stability region retains the random distribution of S^{2-} and I^-, forming a metastable phase labelled α^*-Ag_3SI [17, 21]. On cooling, no further transitions are observed in α^*-Ag_3SI [22] although it reverts to β-Ag_3SI on heating above $\sim$325 K.

Whilst the room temperature ionic conducting properties of Ag_3SI are very impressive ($\sigma \approx 0.008\ \Omega^{-1}\ \mathrm{cm}^{-1}$ and $\sigma \approx 0.3\ \Omega^{-1}\ \mathrm{cm}^{-1}$ for β-Ag_3SI and α^*-Ag_3SI, respectively [22]), their exploitation has been limited by other drawbacks, including the relatively high cost of silver. Nevertheless, the compound has been widely studied as a model superionic system, to investigate the systematic variation of the superionic behaviour on increasing cation density across the series of b.c.c.-structured phases α-AgI $\rightarrow$ α-Ag_3SI $\rightarrow$ β-Ag_2S, in which the number of mobile cations per anion increases from 1 to 1.5 to 2. However, the exact nature of the Ag^+ distribution within the four phases α, α^*, β and γ has been the subject of some debate within the literature [15–21] and this has motivated an extensive study of their crystallographic and transport properties by the authors. In this paper we report structural studies of the four phases of Ag_3SI using powder neutron diffraction.

2. Experimental procedure

The samples used in these experiments were prepared from equimolar mixtures of powdered AgI and Ag_2S, both of stated purity 99.999% and supplied by Johnson-Matthey plc. After grinding, the mixture of the two starting materials was sealed under vacuum in a silica ampoule and placed in a tube furnace at 973(5) K (i.e. within the stability region of the α-phase of Ag_3SI).

After three days the samples were removed from the ampoules, reground and compressed into pellets ∼5 mm in diameter and ∼5 mm in length and then resealed in silica. Following a further three days at 973(5) K some samples were quenched into cold water to form the metastable α^*-phase whilst the remainder were annealed at 473(2) K for prolonged periods of up to three months in order to promote anion ordering and stabilize the β-phase.

The majority of the diffraction experiments were performed using the Polaris powder diffractometer at the ISIS facility, UK [23]. The samples were powdered and then either encapsulated inside silica tubes, of approximate wall thickness 0.5 mm, and heated inside a furnace constructed from a vanadium resistive heating element and heat shields or loaded into a thin-walled vanadium can and mounted on the cold finger of a closed-cycle helium refrigerator. Data for Rietveld profile refinement were collected using detector banks which cover the scattering angles $85^\circ < \pm 2\theta < 95^\circ$ and provide data over the d-spacing range $0.3 \lesssim d$ (Å) $\lesssim 4.3$ with a resolution $\Delta d/d \sim 6 \times 10^{-3}$. Typical counting times were 6–8 hours and the diffraction data were corrected for the effects of neutron absorption within the sample itself [23].

In addition, in order to produce fully corrected total scattering structure factor factors, $F(Q)$, separate measurements of a similar empty can within the CCR and an ampoule within the furnace, an empty CCR and furnace, a standard vanadium rod, a silicon sample and the empty instrument were also made. Data from all the detector banks were corrected and merged in a manner routinely used for the treatment of scattering data from liquid and amorphous samples [24] to produce a normalized differential cross-section, $\mathrm{d}\sigma/\mathrm{d}\Omega$, over the range $0.9 < Q < 20$ Å^{-1} for each temperature.

The total scattering structure factor, $F(Q)$, may be defined in terms of the differential cross-section

$$\frac{1}{N}\frac{\mathrm{d}\sigma}{\mathrm{d}\Omega} = F(Q) + \sum_{i=1}^{n} c_i \bar{b}_i^2$$

where $4\pi \sum_{i=1}^{n} c_i \bar{b}_i^2$ is the total scattering cross-section of the material and the summation is over the n atom types. There are N atoms in the material and c_i is the proportion of atom type i. $F(Q)$ is related to the total radial distribution function, $G(r)$, by the Fourier transform

$$G(r) = \frac{1}{(2\pi)^3 \rho_0} \int_0^\infty 4\pi Q^2 F(Q) \frac{\sin Qr}{Qr}\, \mathrm{d}Q$$

with average atom number density $\rho_0 = N/V$ (in atoms Å^{-3}). $G(r)$ may also be defined in terms of partial radial distribution functions, $g_{ij}(r)$:

$$G(r) = \sum_{i,j=1}^{n} c_i c_j \bar{b}_i \bar{b}_j [g_{ij}(r) - 1] \tag{1}$$

where

$$g_{ij}(r) = \frac{n_{ij}}{4\pi r^2\, \mathrm{d}r\, \rho_j}.$$

The $n_{ij}(r)$ are the number of particles of type j between distances r and $r + \mathrm{d}r$ from a particle of type i and $\rho_j = c_j \rho_0$.

Rietveld profile refinement used the program TF12LS [25], which is based on the Cambridge Crystallographic Subroutine Library [26]. In assessing the relative quality of fits to the experimental data using different structural models, the usual χ^2-statistic is used, defined by

$$\chi^2 = \sum_{N_d} \frac{(I_{obs} - I_{calc})^2}{(\sigma I_{obs})^2} \Big/ (N_d - N_p).$$

N_d is the number of data points used in the fit and N_p is the number of fitted parameters. I_{obs} and I_{calc} are the observed and calculated intensities, respectively, and σI_{obs} is the estimated standard deviation on I_{obs}, derived from the counting statistics. High-resolution powder neutron diffraction data were collected for one phase (γ-Ag_3SI) at 5 K using the HRPD instrument at ISIS [27]. Using the backscattering detector bank ($160^\circ < \pm 2\theta < 176^\circ$), data were collected over the d-spacing range $1.1 \lesssim d$ (Å) $\lesssim 2.9$ with a resolution $\Delta d/d \sim 5 \times 10^{-4}$.

Two-terminal measurements of the ionic conductivity were performed using pelleted samples of ∼5 mm diameter and ∼5 mm in length. These were held between two spring-loaded copper discs within a cell clamped to the cold stage of a closed-cycle refrigerator. Details of this device can be obtained elsewhere [28]. A Solartron S1260 Frequency Response Analyser determined the conventional Z–Z' Bode plot over the frequency range from 0.1 Hz to 10 MHz and the real component of the sample impedance Z_S was determined using software developed in house [28].

3. Results

The normalized structure factors, $F(Q)$, for the four phases of Ag_3SI are illustrated in figure 1. In the case of the data collected from α-Ag_3SI at 569(2) K only ∼8 Bragg peaks are visible but there is significant diffuse scattering observed between the Bragg peaks. In general terms, this is indicative of a highly disordered structure. The $F(Q)$ data for the α^*- and β-phases at ambient temperature appear relatively similar with both showing some diffuse scattering, although the β-phase data contain more Bragg peaks, some of which occur as broad peaks in the α^*-phase (e.g. the 111 reflection at $Q \simeq 2.2$ Å^{-1}). The data collected from γ-Ag_3SI at 10(1) K show Bragg peaks extending to very high Q, suggesting long-range order and, as might be expected, small thermal vibrations. The degree of long-range order within the four phases is also clearly illustrated by the persistence of peaks to high r in their total radial distribution functions $G(r)$ in figure 2. A discussion of the various features shown in figure 2

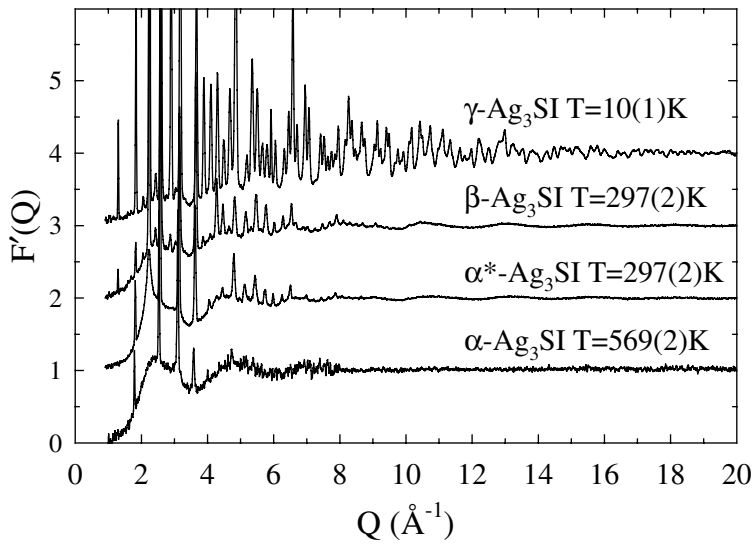

Figure 1. The normalized total scattering structure factor, $F'(Q)$, for the four phases of Ag_3SI. Here $F(Q)$ has been scaled such that $F'(Q) = F(Q)/\sum_{i=1}^{n} c_i \bar{b}_i^2 + 1$.

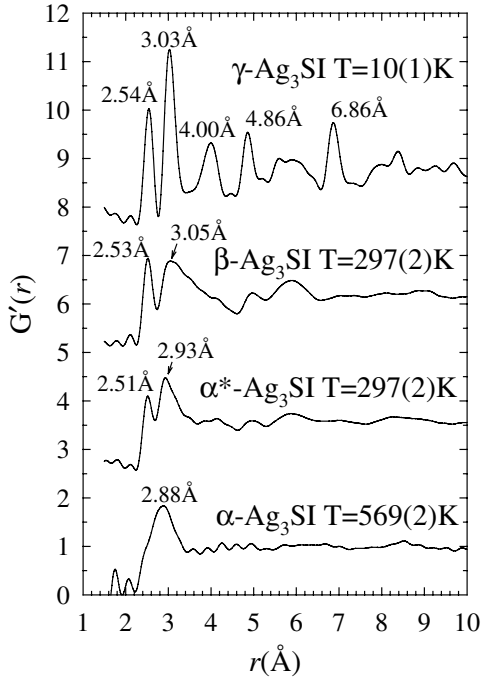

Figure 2. The total radial distribution function, $G'(r)$, for the four phases of Ag_3SI. Here $G(r)$ has been scaled such that $G'(r) - 1 = G(r)/(\sum_{i=1}^{n} c_i \bar{b}_i)^2$.

will be given in section 4, after the following subsections have presented the results obtained for the time-averaged structure determined by least-squares fitting of the Bragg peak data.

3.1. The phase α-Ag_3SI

The observed Bragg peaks from the high-temperature superionic phase α-Ag_3SI are consistent with a body-centred cubic unit cell of dimension ∼4.97 Å. To confirm this we initially perform a so-called 'model-independent' least-squares fit to the diffraction data, which varies the 15 coefficients of a polynomial describing the background (diffuse) scattering, the unit-cell parameter a, a Gaussian peak width parameter and the intensities of the Bragg peaks at d-spacings allowed by space group $Im\bar{3}m$. This procedure does not impose (or provide) any direct structural information concerning the time-averaged location of the ions within the unit cell but it confirms the assignment of the unit cell and space group. In addition, the value of χ^2 obtained ($\chi^2 = 2.20$) gives an estimate of the lowest value that can reasonably be obtained using a structural model.

The models are labelled B to G (with A being the model-independent fit described above) and the results are summarized in table 1. Space group $Im\bar{3}m$ requires the absence of any long-range order of the two cation species and we assume that the 2(a) sites at $0, 0, 0$ and $1/2, 1/2, 1/2$ are both randomly occupied by S^{2-} and I^-. Models B, C and D assume that the three Ag^+ per unit cell are randomly distributed over the 6(b) octahedral sites at $0, 1/2, 1/2$ etc, the 12(d) tetrahedral sites at $1/4, 0, 1/2$ etc and the 24(h) trigonal sites at $x, x, 0$ etc with $x \sim 3/8$, respectively. Of these, model B did not converge satisfactorily, especially when allowing the thermal vibrations of the Ag^+ to vary anisotropically. Model D gave a better fit to

Table 1. The values of the goodness-of-fit parameter χ^2 (see the text) obtained by least-squares fitting of the diffraction data collected from α-Ag_3SI at $T = 569(2)$ K using the structural models A to G. (α-Ag_3SI, $T = 569(2)$ K, $Im\bar{3}m$, S^{2-}/I^- in 2(a) at 0, 0, 0 and 1/2, 1/2, 1/2.)

Model	Description	Ag^+ sites	χ^2
A	Model independent	—	2.28
B	Octahedral sites	6(b) at 0, 1/2, 1/2 etc	~ 3.1
C	Tetrahedral sites	12(d) at 1/4, 0, 1/2 etc	2.52
D	Trigonal sites	24(h) at 0, y, y etc with $y \sim 3/8$	2.14
E	Displaced tetrahedral	24(g) at x, 0, 1/2 etc with $x \sim 0.4$	~ 2.5
F	Octahedral + tetrahedral	6(b) and 12(d)	2.53
G	Tetrahedral + trigonal	12(d) and 24(h)	2.17

the experimental data ($\chi^2 = 2.14$) than model C, with the value of the position parameter x for the Ag^+ site staying (within error) at the value of 3/8 which defines ideal trigonal coordination. Model E places the Ag^+ between the octahedral and tetrahedral interstices in 24(g) positions at x, 0, 1/2 with $x \sim 0.43$. It has been proposed that this site be occupied in samples quenched to room temperature from the α-phase ([17] and see below). However, least-squares fits using this model gave a relatively high value of χ^2 and were rather unstable if the positional parameter x was allowed to vary.

Further, more complex, models allow the simultaneous occupancy of two sites: the octahedral 6(b) and tetrahedral 12(d) sites in model F and the tetrahedral 12(d) and trigonal 24(h) sites in model G. However, neither of these models proved satisfactory. The former gave a high value of χ^2 and the latter produced a physically meaningless (negative) value for the occupancy of the tetrahedral positions. In view of the relatively small number of observed reflections it is unwise to consider more complex structural models of the types proposed previously [16]. Hence, we believe that the best description of the time-averaged structure of the phase α-Ag_3SI has the Ag^+ randomly distributed over the trigonal 24(h) positions (i.e. model D). The quality of the final fit is illustrated in figure 3 and the values of the fitted parameters are listed in table 2. The structure is shown in figure 4 and illustrates the significant anisotropy in the thermal vibrations.

3.2. The phase α^*-Ag_3SI

The procedure to determine the crystal structure of the quenched α^*-phase initially follows that described above for the high-temperature α-phase and is summarized in table 3. A model-independent fit to the data collected at 297(2) K (model A) confirmed that the material adopts the same $Im\bar{3}m$ space group as α-Ag_3SI and we therefore distribute the S^{2-} and I^- randomly over the 2(a) sites at 0, 0, 0 and 1/2, 1/2, 1/2. Models B, C, D constrain the Ag^+ to be randomly distributed over the 6(b) octahedral, 12(d) tetrahedral and 24(h) trigonal positions though, as illustrated in table 3, all give a relatively poor fit to the data ($\chi^2 > 4$). Similarly, attempts to locate the cations in 24(g) positions between the octahedral and tetrahedral positions (model E, with $x \sim 0.37$) and to distribute the cations simultaneously over the octahedral and tetrahedral sites (model F) did not improve the situation significantly.

Previous workers have proposed that the majority of the cations occupy the 24(g) positions but with a significant proportion also located in linearly coordinated sites 8(c) at 1/4, 1/4, 1/4 etc [16, 17]. This situation is described by model G and provides a good fit to the diffraction data with a relatively good value of $\chi^2 = 2.80$. However, it is important to consider whether this model makes physical sense. In particular, those cations located in the 8(c) positions will

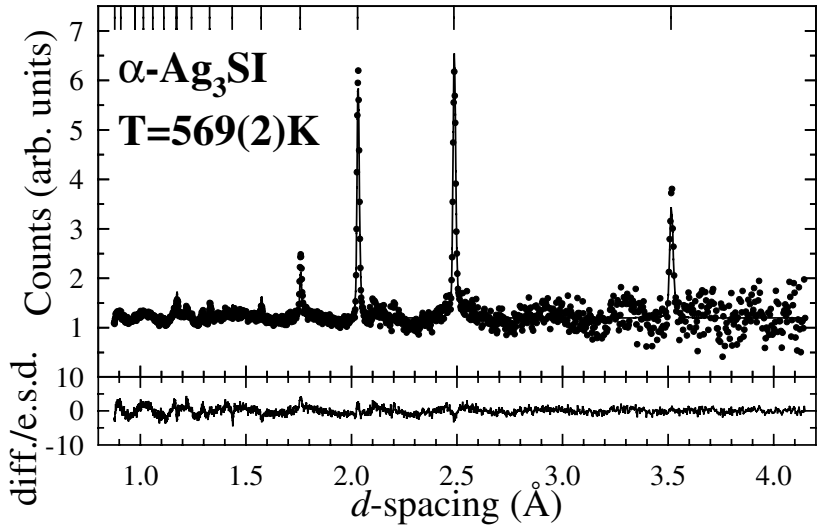

Figure 3. The final least-squares fit to the powder neutron diffraction data collected from α-Ag_3SI at $T = 569(2)$ K. The dots are the experimental data points and the solid line is the profile calculated using the parameters listed in table 2. The lower trace shows the difference (measured minus calculated) divided by the estimated standard deviation on the experimental data points. The tick marks along the top of the figure denote the calculated positions of all the symmetry-allowed Bragg reflections.

Table 2. Summary of the results of the least-squares fit to the diffraction data collected from α-Ag_3SI at $T = 569(2)$ K.

Space group	$Im\bar{3}m$
Lattice parameter	$a = 4.97727(14)$ Å
S^{2-}/I^{-} in 2(a) at 0, 0, 0	
Isotropic thermal parameter	$B_{iso} = 6.3(3)$ Å^2
Ag^{-} in 24(h) at $x, x, 0$	
Positional parameter	$x = 0.375(2)$
Anisotropic thermal parameters	$B_{11} = B_{22} = 11.1(8)$ Å^2
	$B_{33} = 8.2(9)$ Å^2
	$B_{12} = 2.7(6)$ Å^2
Goodness-of-fit	$\chi^2 = 2.14$
Weighted R-factor	$R_w = 1.36\%$
Expected R-factor	$R_{exp} = 0.93\%$
Number of data points	$N_d = 3083$
Number of Bragg peaks	$N_p = 36$
Number of fitted parameters	$N_f = 34$

have two anions located at a distance $\sqrt{3}a/4 \sim 2.13$ Å. Even in the most favourable case in which the neighbouring anions are the smaller S^{2-} species, this distance is significantly shorter than the sum of the ionic radii ($r_{I^-} = 2.20$ Å, $r_{S^{2-}} = 1.84$ Å and $r_{Ag^+} = 0.67$ Å so $r_{S^{2-}} + r_{Ag^+} = 2.51$ Å [29]). Furthermore, the thermal vibrations of the linear coordinated cations are found to be extremely large and anisotropic, forming a disc perpendicular to the $\langle 111 \rangle$ directions of the cation–anion bond. This is suggestive of additional scattering density

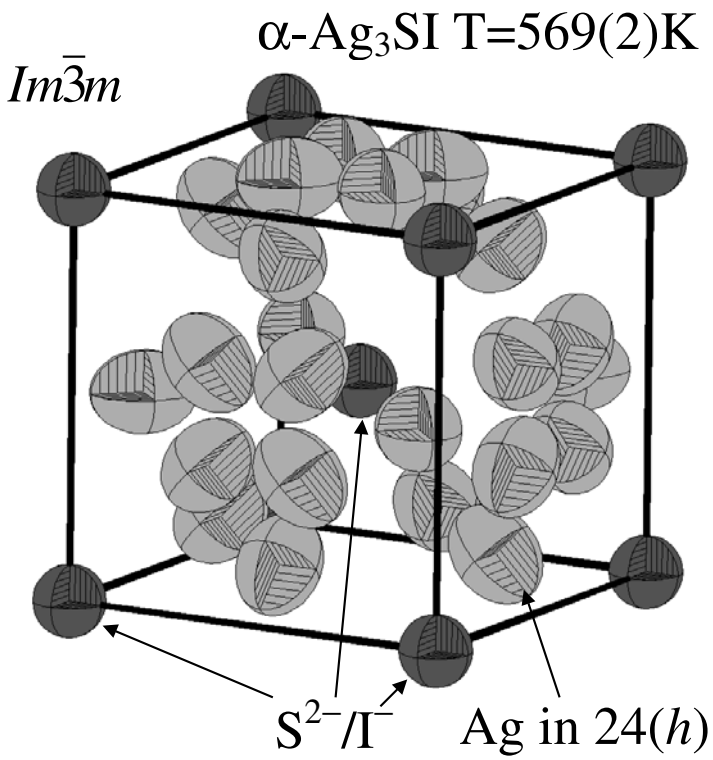

Figure 4. A schematic diagram of the structure of α-Ag_3SI at $T = 569(2)$ K.

Table 3. The values of the goodness-of-fit parameter χ^2 (see the text) obtained by least-squares fitting of the diffraction data collected from α^*-Ag_3SI at $T = 297(2)$ K using the structural models A to H. ($Im\bar{3}m$, S^{2-}/I^- in 2(a) at 0, 0, 0 and 1/2, 1/2, 1/2.)

Model	Description	Ag^+ sites	χ^2
A	Model independent	—	2.12
B	Octahedral sites	6(b) at 0, 1/2, 1/2 etc	4.14
C	Tetrahedral sites	12(d) at 1/4, 0, 1/2 etc	6.45
D	Trigonal sites	24(h) at 0, y, y etc with $y \sim 3/8$	4.96
E	Displaced tetrahedral	24(g) at x, 0, 1/2 etc with $x \sim 0.4$	4.01
F	Octahedral + tetrahedral	6(b) and 12(d)	4.09
G	Displaced tetrahedral + linear	24(g) and 8(c) at 1/4, 1/4, 1/4 etc	2.80
H	Displaced tetrahedral + displaced linear	24(g) and 48(i) at 1/4, y, $1/2 - y$ etc	2.60

located away from the linear coordinated position and we therefore consider displacements of the 8(c) sites in ⟨100⟩, ⟨110⟩ and ⟨111⟩ directions. Of these, only the ⟨110⟩ case is found to improve χ^2 significantly (model H), with the cations distributed in 48(i) sites at 1/4, y, $1/2-y$ etc with $y = 0.148(3)$ and a cation–anion distance of 2.25 Å, although, as we discuss below, this is probably still too short to be physical. As illustrated in figure 5, the refined value of the positional parameter places these cations close to the mid-point between the linear 1/4, 1/4, 1/4 and tetrahedral 1/4, 1/2, 0 positions. The resultant fit is illustrated in figure 6 and a summary of the fitted parameters is given in table 4.

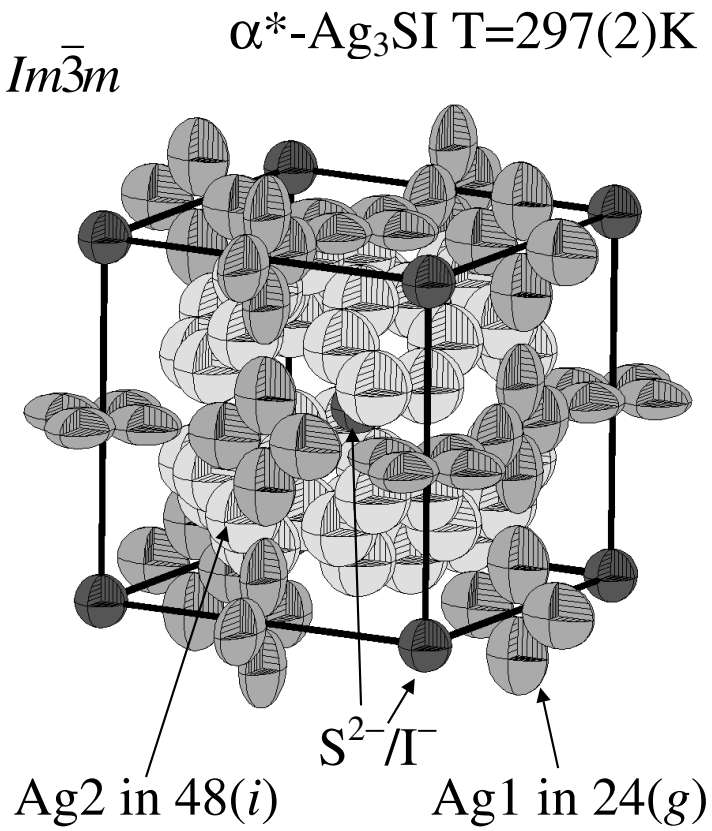

Figure 5. A schematic diagram of the structure of α^*-Ag_3SI at $T = 297(2)$ K.

3.3. The phase β-Ag_3SI

The diffraction pattern from β-Ag_3SI can be completely indexed using a cubic unit cell of comparable dimensions to that used for the α^*-phase. However, as reported by previous studies [16–18], the presence of long-range order of the two anion species lowers the symmetry from $Im\bar{3}m$ to $Pm\bar{3}m$. The latter space group is, therefore, used for the model-independent fit to the diffraction data collected at 297(2) K (model A). As shown in the summary table 5, this procedure gives a good fit to the data and for the remainder of the fits we place the S^{2-} and I^- in the 1(a) sites at 0, 0, 0 and the 1(b) sites at $1/2$, $1/2$, $1/2$, respectively. The loss of the body-centre symmetry operation causes the six octahedral sites to form two inequivalent sets of three positions, in 3(d) at 0, 0, $1/2$ etc and 3(c) at $1/2$, $1/2$, 0 etc. Model B distributes the Ag^+ randomly over all these octahedral positions, such that each site has a mean occupancy of $1/2$. However, this model does not provide an acceptable fit to the data and does not converge satisfactorily if the thermal vibration parameters are varied. It is important to note that the 3(d) and 3(c) octahedral sites are both somewhat distorted, with four anions at a distance $a/\sqrt{2}$ and a further two at a shorter distance of $a/2$. As a result, the 3(d) sites are likely to be favoured over the 3(c) ones because they have four of the larger I^- anions at the longer distance and two of the smaller S^{2-} species at the closer contact, rather than the reverse. Model C therefore places all the cations in the 3(d) sites, forming an ordered (anti-) perovskite structure, and resulting in a moderately good fit to the data. Attempts to constrain the cations to occupy the tetrahedral

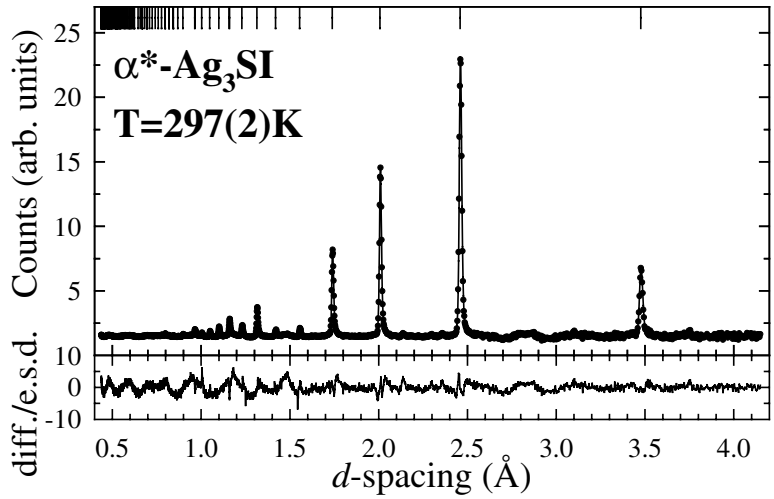

Figure 6. The final least-squares fit to the powder neutron diffraction data collected from α^*-Ag_3SI at $T = 297(2)$ K. The dots are the experimental data points and the solid line is the profile calculated using the parameters listed in table 4. The lower trace shows the difference (measured minus calculated) divided by the estimated standard deviation on the experimental data points. The tick marks along the top of the figure denote the calculated positions of all the symmetry-allowed Bragg reflections.

Table 4. Summary of the results of the least-squares fit to the diffraction data collected from α^*-Ag_3SI at $T = 297(2)$ K.

Space group	$Im\bar{3}m$
Lattice parameter	$a = 4.92385(3)$ Å
S^{2-}/I^- in 2(a) at 0, 0, 0	
Isotropic thermal parameter	$B_{iso} = 4.17(4)$ Å^2
Ag1 in 24(g) at x, 0, 1/2	
Positional parameter	$x = 0.3699(4)$
Anisotropic thermal parameters	$B_{11} = 9.2(3)$ Å^2
	$B_{22} = 2.2(1)$ Å^2
	$B_{33} = 6.6(3)$ Å^2
Site population	$m_{Ag1} = 2.38(3)$
Ag2 in 48(i) at 1/4, y, 1/2 − y	
Positional parameter	$y = 0.148(3)$
Isotropic thermal parameter	$B_{iso} = 8.4(7)$ Å^2
Site population	$m_{Ag2} = 0.62(3)$
Goodness-of-fit	$\chi^2 = 2.60$
Weighted R-factor	$R_w = 1.66\%$
Expected R-factor	$R_{exp} = 1.03\%$
Number of data points	$N_d = 4462$
Number of Bragg peaks	$N_p = 97$
Number of Fitted parameters	$N_f = 42$

positions (12(h) sites at x, 1/2, 0 with $x = 1/4$) using model D proved unsuccessful (diverging χ^2). However, allowing the positional parameter x of the 12(h) site to vary in model E produced

Table 5. The values of the goodness-of-fit parameter χ^2 (see the text) obtained by least-squares fitting of the diffraction data collected from β-Ag_3SI at $T = 297(2)$ K using the structural models A to F. The ? indicates that the fit diverged. ($Pm\bar{3}m$, S^{2-} in 1(a) at 0, 0, 0, I^- in 1(b) at 1/2, 1/2, 1/2.)

Model	Description	Ag^+ sites	χ^2
A	Model independent	—	2.25
B	All octahedral sites	3(c) at 0, 1/2, 1/2 etc and 3(d) at 1/2, 0, 0 etc	50.9
C	'Perovskite' octahedral sites	3(d) at 1/2, 0, 0 etc	4.54
D	Tetrahedral sites	12(h) at x, 1/2, 0 etc with $x = 1/4$	?
E	Displaced tetrahedral	12(h) at x, 1/2, 0 etc with $x \sim 0.1$	4.07
F	Octahedral + displaced tetrahedral	3(d) and 12(h)	8.08

a stable minimum and a good fit with $x = 0.0986(6)$, this position being between the octahedral 3(d) and tetrahedral positions at $x = 0$ and $x = 1/4$, respectively. These displaced tetrahedral sites also give two long cation–I^- and two short cation–S^{2-} contacts and serve to increase the cation–S^{2-} contacts from $a/2$ (2.449 Å) to 2.496 Å and reduce the shortest cation–I^- contacts from $a/\sqrt{2}$ (3.463 Å) to 3.140 Å with respect to the octahedral 3(d) site. Attempts to mimic this behaviour by allowing simultaneous occupancy of the octahedral and tetrahedral positions (model F) gave a somewhat higher value of χ^2 and we therefore conclude that the best description is given by model E. Figures 7 and 8 illustrate the quality of the fit to the diffraction data and the structure of β-Ag_3SI, respectively. The values of the fitted parameters are given in table 6.

Table 6. Summary of the results of the least-squares fit to the diffraction data collected from β-Ag_3SI at $T = 297(2)$ K.

Space group	$Pm\bar{3}m$
Lattice parameter	$a = 4.89727(3)$ Å
I^- in 1(b) at 1/2, 1/2, 1/2	
Isotropic thermal parameter	$B_{iso} = 2.70(3)$ Å^2
S^{2-} in 1(a) at 0, 0, 0	
Isotropic thermal parameter	$B_{iso} = 1.88(4)$ Å^2
Ag^- in 12(h) at x, 1/2, 0	
Positional parameter	$x = 0.0986(6)$
Anisotropic thermal parameters	$B_{11} = 10.0(2)$ Å^2
	$B_{22} = 1.52(5)$ Å^2
	$B_{33} = 7.3(2)$ Å^2
Goodness-of-fit	$\chi^2 = 4.07$
Weighted R-factor	$R_w = 2.12\%$
Expected R-factor	$R_{exp} = 1.05\%$
Number of data points	$N_d = 4474$
Number of Bragg peaks	$N_p = 185$
Number of fitted parameters	$N_f = 30$

3.4. The phase γ-Ag_3SI

Measurements of the ionic conductivity σ of β-Ag_3SI on cooling are illustrated in figure 9. The presence of an abrupt decrease in σ at $T = 156(2)$ K is indicative of the transition to

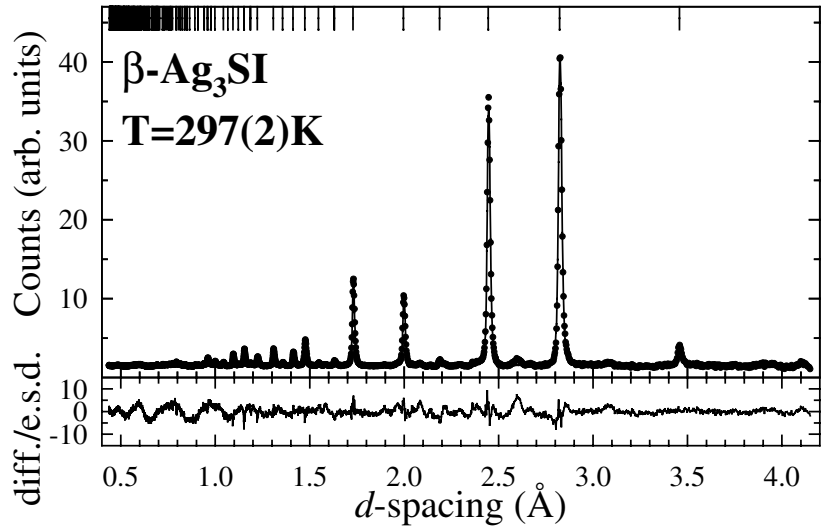

Figure 7. The final least-squares fit to the powder neutron diffraction data collected from β-Ag_3SI at $T = 297(2)$ K. The dots are the experimental data points and the solid line is the profile calculated using the parameters listed in table 6. The lower trace shows the difference (measured minus calculated) divided by the estimated standard deviation on the experimental data points. The tick marks along the top of the figure denote the calculated positions of all the symmetry-allowed Bragg reflections.

the low-temperature γ-phase. Previous diffraction studies of γ-Ag_3SI have proposed that the cubic unit cell undergoes a rhombohedral distortion, though the extent of the distortion along one of the $\langle 111 \rangle$ directions was too small to be resolved experimentally and the interaxial angle α was, within error, equal to 90° [18, 20]. Since the nature of the metric is important in testing and selecting an appropriate model for the crystal structure of γ-Ag_3SI, high-resolution powder neutron diffraction studies were performed of this phase at $T = 5(1)$ K. As illustrated in figure 10, there is a significant broadening of the 'cubic' 111 reflection compared with the 002 peak, which is consistent with a rhombohedral distortion of the unit cell. A model-independent fit to these data gives a value of 0.08(2)° for the distortion, though it is not possible to differentiate between unit cells with $\alpha = 89.92(2)^\circ$ and $\alpha = 90.08(2)^\circ$. Unfortunately, instrumental constraints mean that high-resolution diffraction data could only be collected over a relatively limited d-spacing range and, in particular, the absence of measured peaks at low d-spacing ($d \lesssim 1$ Å) prevents these data from being used for determination of the crystal structure. Instead, we use the medium-resolution (high-intensity) data collected at $T = 10(1)$ K (figure 1) with the interaxial angle α fixed at 90° since the resolution is insufficient to obtain a meaningful fitted value. However, a subsequent fit to the high-resolution data using the structural model determined below gave a good fit to the (limited range) data and showed that the correct unit-cell description has $\alpha = 90.08(2)^\circ$.

The medium-resolution diffraction pattern collected from the phase γ-Ag_3SI at $T = 10(1)$ K resembles that of β-Ag_3SI, with apparently the same primitive cubic unit cell though with significant changes in the intensities of many of the reflections. This is confirmed by the relatively low value of χ^2 provided by the model-independent fit to the diffraction data collected from γ-Ag_3SI using space group $Pm\bar{3}m$ (see table 7). Since the two anion species are ordered over the 0, 0, 0 and 1/2, 1/2, 1/2 sites in β-Ag_3SI it is reasonable to assume that the same is true in γ-Ag_3SI. However, it was not possible to obtain low values of χ^2 with the cations

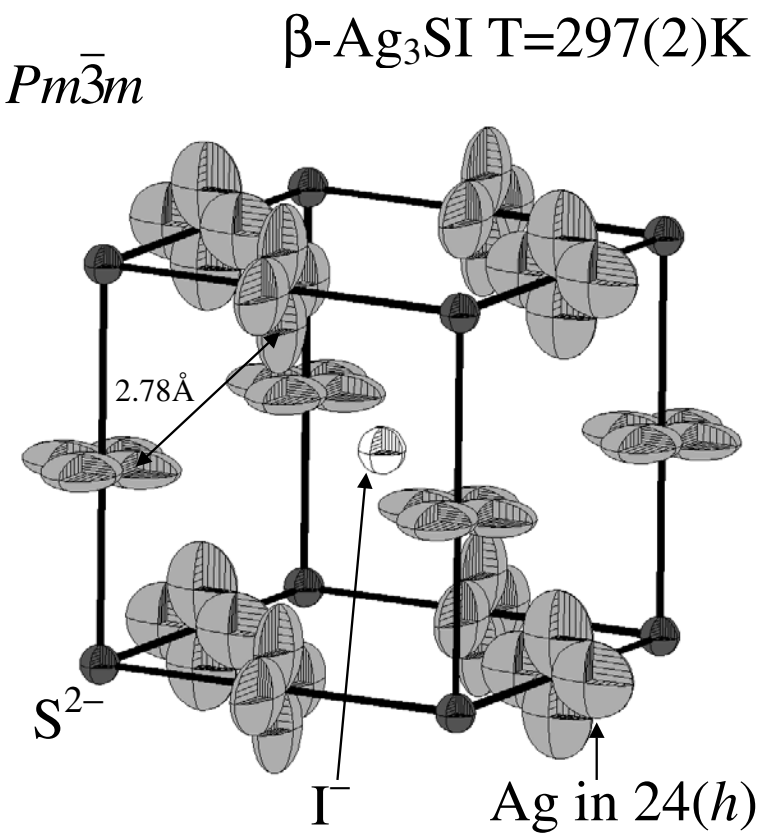

Figure 8. A schematic diagram of the structure of β-Ag_3SI at $T = 569(2)$ K.

distributed over the available octahedral and (displaced) tetrahedral sites. This is illustrated in table 7 by models B and C, the former being an ordered anti-perovskite arrangement with the Ag^+ in octahedral sites and the latter using the 12(h) sites which are occupied in β-Ag_3SI (see above).

To derive the correct structure of γ-Ag_3SI we consider the possibility that the three cations per unit cell become ordered over a subset of the twelve displaced tetrahedral sites occupied in the β-phase. This possibility has been discussed in previous structural studies of γ-Ag_3SI and is clearly consistent with the decrease in the ionic conductivity σ at the $\beta \rightarrow \gamma$ transition (figure 9). However, ordering of the cations requires lowering of the symmetry from cubic to rhombohedral and model D is simply the rhombohedral equivalent of model C. The cations are randomly distributed over all the tetrahedral sites which are in the 12(i) x, y, z general positions of space group $R\bar{3}m$, with $x \sim 0.1$, $y \sim 1/2$ and $z \sim 0$. As might be expected, model D gives a comparable value of χ^2 to model C. Figure 11 illustrates the different ways in which it is possible to order the three Ag^+ over the twelve available displaced tetrahedral positions. In space groups $R3m$, $R32$ and $R\bar{3}$ (models E, F and G, respectively) there are two sets of inequivalent sites, each containing six positions, whilst in the case of $R3$ (model H) there are four inequivalent sets, each one containing three positions. Within the fitting procedure we constrain the positions of the various sets to remain close to the original twelve sites discussed above and constrain the isotropic thermal vibration parameter of all the Ag^+ to be equal.

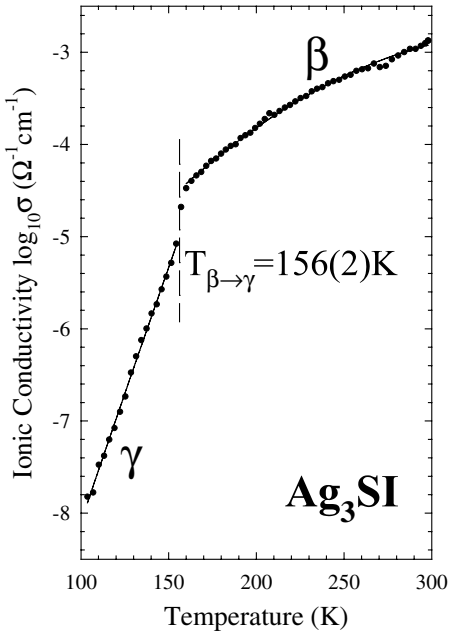

Figure 9. The temperature variation of the ionic conductivity $\log_{10}\sigma$ of Ag_3SI illustrating the discontinuous change at the $\beta \rightarrow \gamma$ transition temperature of $T = 156(2)$ K.

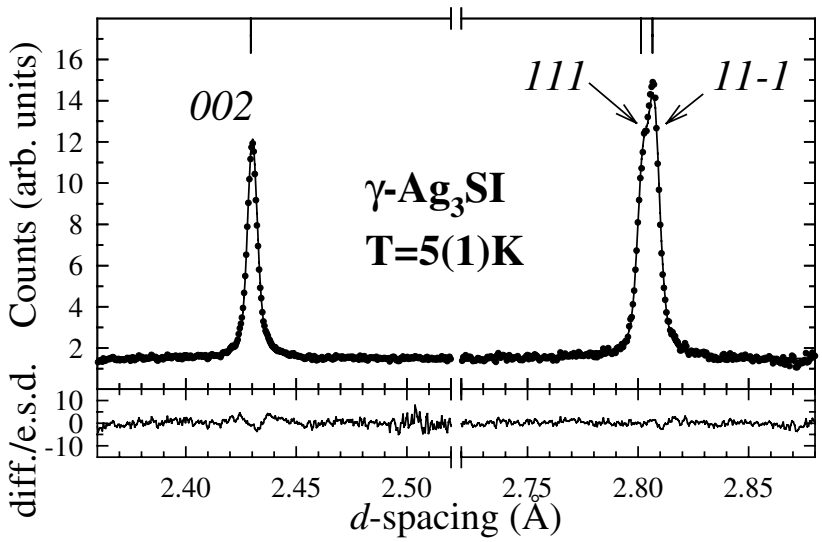

Figure 10. A portion of the least-squares fit to the high-resolution powder neutron diffraction data collected from γ-Ag_3SI at $T = 5(1)$ K. The small rhombohedral distortion ($\alpha = 90.08(2)^\circ$) is observed as an increase in the width of the $111/11\bar{1}$ peak in comparison to 002. The dots are the experimental data points and the solid line is the calculated profile. The lower trace shows the difference (measured minus calculated) divided by the estimated standard deviation on the experimental data points. The tick marks along the top of the figure denote the calculated positions of the Bragg reflections.

Table 7. The values of the goodness-of-fit parameter χ^2 (see the text) obtained by least-squares fitting of the diffraction data collected from γ-Ag_3SI at $T = 10(1)$ K using the structural models A to I. (SG ≡ space group; 'tet.' stands for tetrahedral.)

Model	Description	SG	S^{2-} sites	I^- sites
A	Model independent	—	—	—
B	Octahedral sites	$Pm\bar{3}m$	1(a) at 0, 0, 0	1(b) at 1/2, 1/2, 1/2
C	Tetrahedral sites	$Pm\bar{3}m$	1(a) at 0, 0, 0	1(b) at 1/2, 1/2, 1/2
D	All displaced tet.	$R\bar{3}m$	1(a) at 0, 0, 0	1(b) at 1/2, 1/2, 1/2
E	Two sets of tet. sites	$R3m$	1(a) at x, x, x with $x \sim 0.0$	1(a) at x, x, x with $x = 1/2$
F	Two sets of tet. sites	$R32$	1(a) at 0, 0, 0	1(b) at 1/2, 1/2, 1/2
G	Two sets of tet. sites	$R\bar{3}$	1(a) at 0, 0, 0	1(b) at 1/2, 1/2, 1/2
H	Four sets of tet. sites	$R3$	1(a) at x, x, x with $x \sim 0.0$	1(a) at x, x, x with $x = 1/2$
I	Fully ordered	$R3$	1(a) at x, x, x with $x \sim 0.0$	1(a) at x, x, x with $x = 1/2$

Model	Description	SG	Ag^+ sites	χ^2
A	Model independent	—	—	4.64
B	Octahedral sites	$Pm\bar{3}m$	3(d) at 1/2, 0, 0 etc	~ 300
C	Tetrahedral sites	$Pm\bar{3}m$	12(h) at x, 1/2, 0 etc with $x \sim 0.1$	43.6
D	All displaced tet.	$R\bar{3}m$	12(i) at x, y, z etc, $x \sim 0.1$, $y \sim 1/2$, $z \sim 0$	44.4
E	Two sets of tet. sites	$R3m$	6(c) at x, y, z etc, $x \sim 0.1$, $y \sim 1/2$, $z \sim 0$ 6(c) at x, y, z etc, $x \sim 0.9$, $y \sim 1/2$, $z \sim 0$	40.3
F	Two sets of tet. sites	$R32$	6(f) at x, y, z etc, $x \sim 0.1$, $y \sim 1/2$, $z \sim 0$ 6(f) at x, y, z etc, $x \sim 0.9$, $y \sim 1/2$, $z \sim 0$	50.3
G	Two sets of tet. sites	$R\bar{3}$	6(f) at x, y, z etc, $x \sim 0.1$, $y \sim 1/2$, $z \sim 0$ 6(f) at x, y, z etc, $x \sim 1/2$, $y \sim 0.9$, $z \sim 0$	42.4
H	Four sets of tet. sites	$R3$	3(b) at x, y, z etc, $x \sim 0.1$, $y \sim 1/2$, $z \sim 0$ 3(b) at x, y, z etc, $x \sim 1/2$, $y \sim 0.9$, $z \sim 0$ 3(b) at x, y, z etc, $x \sim 0.9$, $y \sim 1/2$, $z \sim 0$ 3(b) at x, y, z etc, $x \sim 1/2$, $y \sim 0.1$, $z \sim 0$	8.26
I	Fully ordered	$R3$	3(b) at x, y, z etc, $x \sim 1/2$, $y \sim 0.9$, $z \sim 0$	7.40

The occupancies of each of the sets is then allowed to vary (subject to the constraint of three Ag^+ per unit cell) to investigate the possibility of cation ordering. In addition, space groups $R3m$ and $R3$ are polar and allow the S^{2-} sublattice to be displaced in the [111] direction relative to the I^- one. It is clear from table 7 that models E, F and G which occupy six of the twelve available sites do not provide an improved fit. However, model H gives a good fit to the data, with the occupancies of the four 3(b) sets of sites (see table 7) being 0.11(1), 2.78(1), 0.16(1) and −0.05(4). Clearly this model is indicative of strong ordering of the three Ag^+

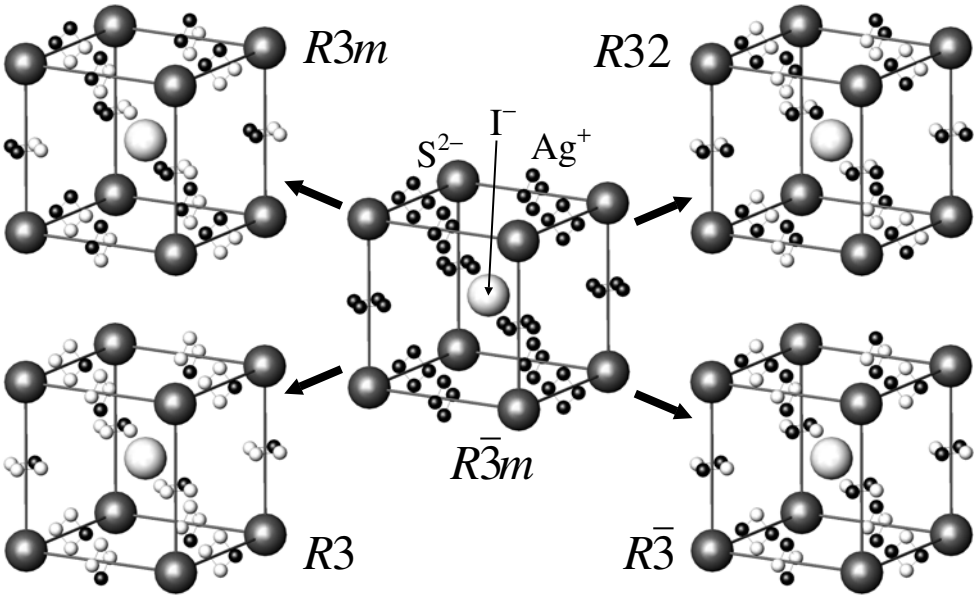

Figure 11. Alternative ordering schemes obtained by distributing the three Ag^+ per unit cell over the twelve available displaced tetrahedral sites in possible structures of the low-temperature γ-Ag_3SI phase.

onto the 3(b) sites at x, y, z with $x \sim 1/2$, $y \sim 0.9$ and $z \sim 0$. Model I is a more simplified version of model H, which assumes full occupancy of these three sites and zero occupancy of the other three sets. Removing the option to vary the site occupancies results in a significantly better constrained fit and it is possible to vary the anisotropic thermal vibration parameters of the Ag^+ (see figure 12). This results in a somewhat lower value of χ^2 and gives the final set of parameters listed in table 8. The fit to the data is illustrated in figure 13.

4. Discussion

The results presented in the previous section are the first in an extensive study of the structure–property relationships in Ag_3SI. This study will include a more detailed temperature-dependent powder neutron diffraction study of the $\gamma \leftrightarrow \beta$ transition, further impedance spectroscopy studies of the behaviour of the ionic conductivity and molecular dynamics simulations to probe the microscopic nature of the conduction mechanism. In addition, a detailed analysis of the total scattering ($F(Q)$ in figure 1) is in progress using reverse Monte Carlo methods and will be presented in a future publication. For the moment we will consider only the structural properties of the four phases of Ag_3SI. In this section we compare the structural information obtained in this work with the previous studies. Where necessary, the crystallographic origin has been shifted to conform to that used in this work, which corresponds to the conventional description of the perovskite structure in which the smaller S^{2-} species is at (or near) 0, 0, 0. We also attempt to reconcile the time-averaged ionic distributions within the unit cell obtained from the least-squares fitting to the Bragg diffraction data (tables 2, 4, 6 and 8) with the total radial distribution function $G(r)$ (figure 2) obtained by Fourier transform of the normalized total scattering $F(Q)$ (figure 1).

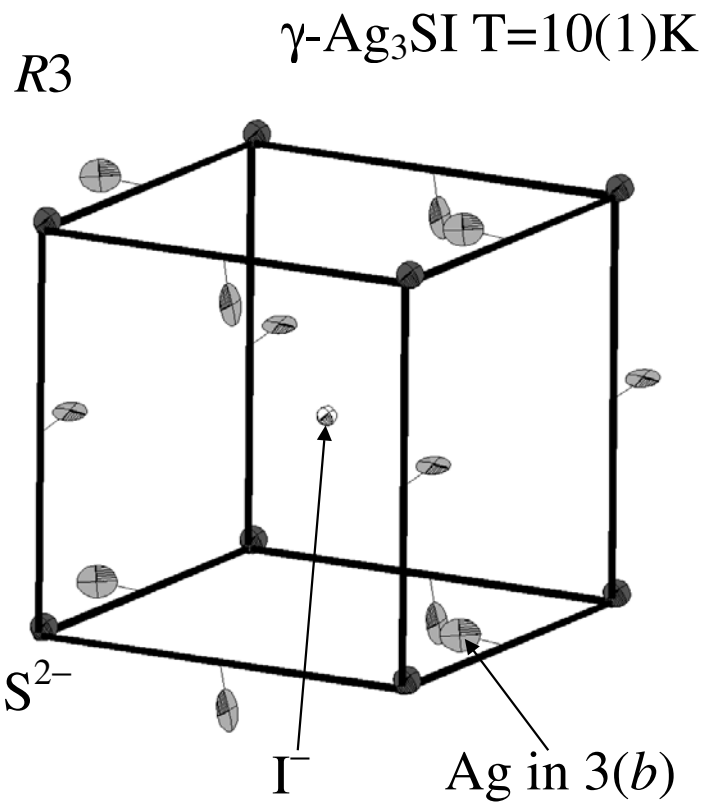

Figure 12. A schematic diagram of the structure of γ-Ag_3SI at $T = 10(1)$ K.

The $G(r)$ data presented in figure 2 represent the total radial distribution function for all the ionic species. However, the contribution to $G(r)$ from each species pair is scaled by their coherent scattering lengths, $\bar{b}$, and proportions, c (see equation (1)). For the three ionic species present in Ag_3SI we have $\bar{b} = 6.02$ fm and $c = 0.6$ for Ag^+, $\bar{b} = 2.85$ fm and $c = 0.2$ for S^{2-} and $\bar{b} = 5.28$ fm and $c = 0.2$ for I^-. As a consequence, Ag^+–Ag^+ correlations will be the dominant constituent of $G(r)$, though Ag^+–I^- and Ag^+–S^{2-} contributions are also likely to be observed. Correlations between the anions are likely to be insignificant, due largely to their lower proportions c. In the case of Bragg scattering, the time-averaged structure of the unit cell describes the distribution of Ag^+ in terms of one, or more, fractionally occupied crystallographic sites (except in the case of the fully ordered γ-Ag_3SI). However, many of these sites are situated too close to each other to be simultaneously occupied. On these geometric grounds we would not expect simultaneous occupancy of Ag^+ interstitial sites separated by less than twice the ionic radius of Ag. In fact, the $G(r)$ data in figure 2 show no peaks less than ∼2.5 Å.

The structural model proposed here for α-Ag_3SI differs somewhat from those proposed previously [15–17], in which the Ag^+ are found to predominantly occupy the octahedral and/or tetrahedral positions, implying that the Ag^+ diffusion pathways are in ⟨100⟩ directions. Unfortunately, the information provided by the $G(r)$ data is relatively limited, with a shoulder at ∼2.60 Å and a peak at 2.88 Å as the only significant features. On the basis of the results of the least-squares analysis of the Bragg diffraction data (table 2) it is possible to calculate

Table 8. Summary of the results of the least-squares fit to the diffraction data collected from γ-Ag_3SI at $T = 10(1)$ K.

Space group	$R3$
Lattice parameters	$a = 4.86728(2)$ Å
	$\alpha = 90^\circ$ (fixed; see the text)
I^- in 1(a) at x, x, x	
Positional parameter	$x = 1/2$ (fixed)
Isotropic thermal parameter	$B_{iso} = 0.44(5)$ Å^2
S^{2-} in 1(a) at x, x, x	
Positional parameter	$x = 0.0319(5)$
Isotropic thermal parameter	$B_{iso} = 0.86(6)$ Å^2
Ag^- in 3(b) at x, y, z	
Positional parameters	$x = 0.5300(5)$
	$y = 0.8895(4)$
	$z = 0.0175(6)$
Anisotropic thermal parameters	$B_{11} = 0.09(4)$ Å^2
	$B_{22} = 2.07(4)$ Å^2
	$B_{33} = 1.22(4)$ Å^2
	$B_{12} = 0.11(7)$ Å^2
	$B_{12} = -0.17(5)$ Å^2
	$B_{12} = -0.31(6)$ Å^2
Goodness-of-fit	$\chi^2 = 7.40$
Weighted R-factor	$R_w = 3.78\%$
Expected R-factor	$R_{exp} = 1.39\%$
Number of data points	$N_d = 4063$
Number of Bragg peaks	$N_p = 1100$
Number of fitted parameters	$N_f = 35$

the distances between the trigonal sites as being 1.24 Å, 1.53 Å, 1.76 Å, 2.64 Å, 2.92 Å and 3.05 Å. Ignoring the (weaker) Ag^+–anion correlations it is plausible to suggest that correlations comprising the latter three distances are present in α-Ag_3SI, though the high degree of dynamic disorder makes it difficult to conclusively assign these.

In the case of α^*-Ag_3SI, the 24(g) sites are also found by Cho *et al* [17] to be predominantly occupied. However, previous suggestions that a proportion of the cations are located in the linearly coordinated 8(c) sites at 1/4, 1/4, 1/4 [16, 17] are questionable because it would imply Ag^+–anion distances of only ∼2.13 Å along the body diagonal. Even if this Ag2 site were only occupied in cases where the terminal anions were the smaller S^{2-} species, this must be questioned on physical grounds because $r_{Ag^+} + r_{S^{2-}} = 2.51$ Å. In this work, the displacement of the additional cations in ⟨110⟩ directions away from the 8(c) sites and into 48(i) positions implies that the $Ag2^+$–anion distance is somewhat longer at 2.25 Å, although this is still probably too short to be physical. Since the quenching process arrests the formation of anion-ordered β-Ag_3SI, it might be expected that there is local ordering of S^{2-} and I^- in α^*-Ag_3SI. This is suggested by the presence of a broad diffuse peak in α^*-Ag_3SI at the same position as the b.c.c.-forbidden 111 reflection in β-Ag_3SI (see figure 1). Diffraction measurements on a single crystal of α^*-Ag_3SI confirm that this broad diffuse peak in $F(Q)$ is indeed centred on the position of the 111 reciprocal-lattice point (see figure 14). Indeed, other, weaker broad peaks are also observed at (for example) 001, 003 and 113, confirming that there is anion ordering over a short length scale in α^*-Ag_3SI. This cannot be treated easily using an average

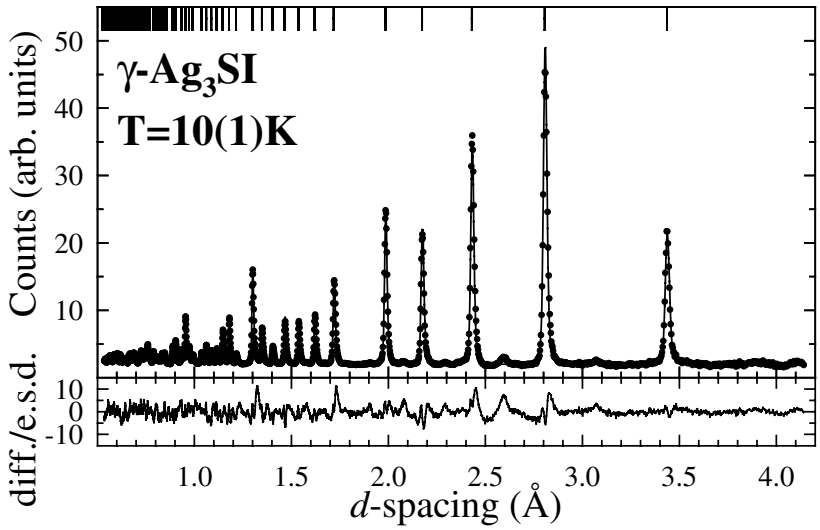

Figure 13. The final least-squares fit to the powder neutron diffraction data collected from γ-Ag_3SI at $T = 10(1)$ K. The dots are the experimental data points and the solid line is the profile calculated using the parameters listed in table 8. The lower trace shows the difference (measured minus calculated) divided by the estimated standard deviation on the experimental data points. The tick marks along the top of the figure denote the calculated positions of all the symmetry-allowed Bragg reflections.

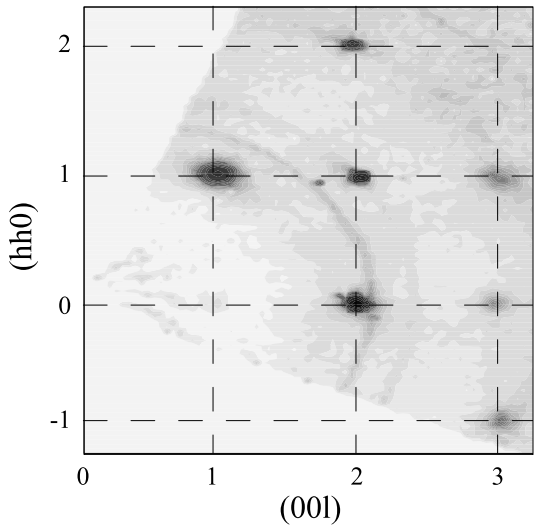

Figure 14. The $1\bar{1}0$ reciprocal-lattice plane of α^*-Ag_3SI at room temperature from a small single crystal measured on the single-crystal neutron diffractometer, SXD, at ISIS. The plot shows resolution-limited b.c.c.-allowed Bragg reflections together with weak broadened peaks at b.c.c.-forbidden reciprocal-lattice points. Weak aluminium powder lines can also be observed in the diffuse background [34].

structure in space group $Im\bar{3}m$ and it is not surprising that the Rietveld refined structure is not altogether satisfactory.

Since, in the average structure, only ∼20% of the Ag^+ are located in the 48(i) sites, it is reasonable to assume that only correlations involving the Ag1 (24(g)) sites need be considered when comparing with $G(r)$. In addition to four short (physically unrealistic) $Ag1^+$–$Ag1^+$ contacts (0.91 Å, 1.18 Å, 1.28 Å, 1.93 Å) there are additional intersite distances of 2.46 Å, 2.58 Å, 2.62 Å, 3.12 Å and 3.16 Å. Clearly, the shorter of these could reasonably account for the first peak in the $G(r)$ at 2.51 Å, though the origin of the second maximum at 2.93 Å is unclear. There could also be a contribution from Ag^+–anion contacts, which are calculated to be 2.54 Å and 3.06 Å. A possible explanation is provided by the discussion of Didisheim *et al* [16] and Hoshino *et al* [21]. They argue that the displaced tetrahedral site in 24(g) is, in fact, a spatial average of a number of closely spaced sites in this region of the unit cell. This arises because, within the disordered anion sublattice, each tetrahedral site can be locally coordinated by a different combination of I^- and S^{2-} (i.e. I_4, S_4, I_3S, S_3I and S_2I_2 tetrahedra). Since the S^{2-} and I^- are of different size it follows that the most favoured central location within each tetrahedron depends on the identity of the anions at each vertex and their configuration. On these grounds a number of sites in 12(d), 48(i), 48(j) and 24(g) positions of space group $Im\bar{3}m$ were identified [16, 21]. Clearly, this structural model is too complex to fit the experimental Bragg diffraction data as not all types of tetrahedron may be occupied to the same extent. It might, for example, be reasonable to assume that locally the Ag^+ prefer to sit in I_2S_2 tetrahedra, since this is their coordination within the stable phase β-Ag_3SI (see figure 8). However, to resolve this issue, reverse Monte Carlo and molecular dynamics studies of α^*-Ag_3SI will shortly be performed and the results presented in a future publication.

For β-Ag_3SI there is complete agreement between our work and the three previous diffraction studies [16–18], which all report occupancy of the 12(h) sites. The ordering of the two anion species and the single occupied Ag^+ site make the interpretation of the $G(r)$ data in figure 2 more straightforward. Two very short Ag^+–Ag^+ contacts at 0.68 Å and 0.97 Å correspond to distances within the cluster of four sites illustrated in figure 8 and clearly these are not simultaneously occupied. In addition, the absence of a peak in $G(r)$ at ∼2.78 Å suggests that there is a degree of correlation between the displacements of the Ag^+ in neighbouring clusters, such that they do not simultaneously move towards one another and the only distances occupied are those greater than ∼3.00 Å. This can be considered as a precursor towards the situation in γ-Ag_3SI, in which the Ag^+ order in a cooperative manner onto a subset of the displaced tetrahedral positions. The first peak in $G(r)$ at 2.53 Å corresponds to that calculated for Ag^+–S^{2-} (2.50 Å) whilst the Ag^+–I^- contact at 3.14 Å is likely to contribute to the shoulder on the high-Q side of the second peak.

The structural model determined in this work for the low-temperature phase γ-Ag_3SI is broadly the same as that published previously [18, 20]. However, in this work we have been able to quantify the extent of the rhombohedral distortion as $0.08(2)^\circ$ at $T = 5(1)$ K. The first three peaks in the $G(r)$ are observed at 2.54 Å, 3.03 Å and 4.00 Å and the first can be interpreted as a combination of the two Ag^+–S^{2-} contacts at 2.52 Å and 2.54 Å. The second is predominantly due to Ag^+–Ag^+ contacts of 3.01 Å and 3.11 Å (plus a smaller component due to Ag^+–I^- distances of 3.02 Å and 3.16 Å) and the third arises from Ag^+–Ag^+ distances of 3.97 Å and 4.04 Å. As discussed above, the γ-Ag_3SI arrangement can be derived from that of β-Ag_3SI by ordering of the three Ag^+ per unit cell over the twelve displaced octahedral positions, coupled with a slight displacement (∼0.3 Å) of the S^{2-} along a ⟨111⟩ direction. The presence of this displacement suggests that γ-Ag_3SI is ferroelectric, in a manner similar to that observed in rhombohedrally distorted perovskites such as $Pb(Zr_{1-x}Ti_x)O_3$ [30] and $LiNbO_3$ [31]. However, reliable measurements of the dielectric properties of γ-Ag_3SI are not possible owing to its relatively high ionic conductivity [32]. Finally, it is interesting to note that a similar structure is found for the compound Ni_3S_2, though the presence of two identical

anions and a simpler distortion of the cations away from the octahedral positions allow the space group to be $R32$ [33]. At ~830 K Ni_3S_2 undergoes a transition to a superionic phase, though this is believed to be based on an f.c.c., rather than b.c.c., immobile S^{2-} sublattice [33].

5. Conclusions

It is clear that the arrangement of the ions within the α-, α^*-, β- and γ-modifications of Ag_3SI are closely related but that the preferred sites occupied by the Ag^+ are somewhat different. In addition to the effect of temperature, this is a direct consequence of the degree of long-range order of the two anion species. In this context, Ag_3SI is an extremely interesting material to study because it is possible to form room temperature modifications which are anion ordered (β) and disordered (α^*). The interrelationship between the degree of order on the anion and cation sublattices and their influence on the ionic conductivity will be the subject of future papers reporting the results of temperature-dependent powder neutron diffraction studies, impedance spectroscopy studies of the conduction properties and molecular dynamics simulations of the ionic diffusion mechanism(s). Such information is of wider relevance in optimizing the ionic conduction properties of other perovskite-related oxide and halide solid electrolytes.

Acknowledgments

The work presented in this paper forms part of a wider project investigating the structural properties of superionic conductors funded by the Engineering and Physical Sciences Research Council (reference GR/M38711).

References

[1] Chandra S 1981 *Superionic Solids. Principles and Applications* (Amsterdam: North-Holland)
[2] Nield V M and Hayes W 1995 *Defect Diffusion Forum* **125+126** 37
[3] Wright A F and Fender B E F 1977 *J. Phys. C: Solid State Phys.* **10** 2261
[4] Nield V M, Keen D A, Hayes W and McGreevy R L 1993 *Solid State Ion.* **66** 247
[5] Nield V M, McGreevy R L, Keen D A and Hayes W 1994 *Physica* B **202** 159
[6] Cava R J, Reidinger F and Wuensch B J 1980 *J. Solid State Chem.* **31** 69
[7] Rino J P, Hornos Y M M, Antonio G A, Ebbsjö I, Kalia R K and Vashishta P 1988 *J. Chem. Phys.* **89** 7542
[8] Schneider J and Schulz H 1993 *Z. Kristall.* **203** 1
[9] Keen D A and Hull S 1998 *J. Phys.: Condens. Matter* **10** 8217
[10] Hull S and Keen D A 1996 *J. Phys.: Condens. Matter* **8** 619
[11] Hull S, Keen D A, Hayes W and Gardner N J G 1998 *J. Phys.: Condens. Matter* **10** 10 941
[12] Reuter B and Hardel K 1965 *Z. Anorg. Allg. Chem.* **340** 158
[13] Reuter B and Hardel K 1965 *Z. Anorg. Allg. Chem.* **340** 168
[14] Reuter B and Hardel K 1966 *Ber. Bunsenges. Phys. Chem.* **70** 82
[15] Perenthaler E and Schulz H 1981 *Solid State Ion.* **2** 43
[16] Didisheim J-J, McMullan R K and Wuensch B J 1986 *Solid State Ion.* **18+19** 1150
[17] Cho N, Kikkawa S, Kanamaru F and Yoshiasa A 1994 *Solid State Ion.* **68** 57
[18] Hoshino S, Sakuma T and Fujii Y 1979 *J. Phys. Soc. Japan* **47** 1252
[19] Hoshino S, Sakuma T and Fujii Y 1978 *J. Phys. Soc. Japan* **45** 705
[20] Perenthaler E, Schulz H and Beyeler H U 1981 *Acta Crystallogr.* B **37** 1017
[21] Hoshino S, Shapiro S M, Fujishita H and Sakuma T 1988 *J. Phys. Soc. Japan* **57** 4199
[22] Chiodelli G, Magistris A and Schiraldi A 1979 *Z. Phys. Chem., NF* **118** 177
[23] Hull S, Smith R I, David W I F, Hannon A C, Mayers J and Cywinski R 1992 *Physica* B **180+181** 1000
[24] Howe M A, McGreevy R L and Howells W S 1989 *J. Phys.: Condens. Matter* **1** 3433
[25] David W I F, Ibberson R M and Matthewman J C 1992 *Rutherford Appleton Laboratory Report* RAL-92-032
[26] Brown P J and Matthewman J C 1987 *Rutherford Appleton Laboratory Report* RAL-87-010
[27] Ibberson R M, David W I F and Knight K S 1992 *Rutherford Appleton Laboratory Report* RAL-92-031

[28] Gardner N J G, Hull S, Keen D A and Berastegui P 1998 *Rutherford Appleton Laboratory Report* RAL-TR-1998-032
[29] Shannon R D 1976 *Acta Crystallogr.* A **32** 751
[30] Glazer A M, Mabud S A and Clarke R 1978 *Acta Crystallogr.* B **34** 1060
[31] Abrahams S C and Marsh P 1986 *Acta Crystallogr.* B **42** 61
[32] Hoshino S, Fujishita H, Takashige M and Sakuma T 1981 *Solid State Ion.* **3+4** 35
[33] Fjellvåg H and Andersen A 1994 *Acta Chem. Scand.* **48** 290
[34] Keen D A and Hull S 1999 private communication